ARTICLE

doi:10.1038/nature09423

The Ndc80 kinetochore complex forms oligomeric arrays along microtubules

Gregory M. Alushin[1], Vincent H. Ramey[1], Sebastiano Pasqualato[2], David A. Ball[3], Nikolaus Grigorieff[4], Andrea Musacchio[2,5] & Eva Nogales[3,6]

The Ndc80 complex is a key site of regulated kinetochore–microtubule attachment (a process required for cell division), but the molecular mechanism underlying its function remains unknown. Here we present a subnanometre-resolution cryo-electron microscopy reconstruction of the human Ndc80 complex bound to microtubules, sufficient for precise docking of crystal structures of the component proteins. We find that the Ndc80 complex binds the microtubule with a tubulin monomer repeat, recognizing α- and β-tubulin at both intra- and inter-tubulin dimer interfaces in a manner that is sensitive to tubulin conformation. Furthermore, Ndc80 complexes self-associate along protofilaments through interactions mediated by the amino-terminal tail of the NDC80 protein, which is the site of phospho-regulation by Aurora B kinase. The complex's mode of interaction with the microtubule and its oligomerization suggest a mechanism by which Aurora B could regulate the stability of load-bearing kinetochore–microtubule attachments.

The Ndc80 complex is a member of the conserved KMN kinetochore network, which also includes the Knl-1 and Mis12 complexes[1]. The Ndc80 complex is the key site for kinetochore–microtubule attachment[1–3] and a landing pad for the spindle assembly checkpoint[4–6]. Although extensively characterized genetically[7,8] and biochemically[1–3,9,10], the mechanisms by which the Ndc80 complex effects and coordinates these activities remain elusive.

The complex is an elongated, 57-nm heterotetramer composed of NDC80 (also known as HEC1), NUF2, SPC24 and SPC25, each having a globular domain connected to a coiled-coil that mediates dimerization: SPC24 with SPC25, and NDC80 with NUF2 (refs 9–12). Tetramerization via the dimerized coiled-coils[9,10] results in a dumbbell architecture, with the SPC24–SPC25 globular head at one end mediating kinetochore association[1,3], and the NDC80–NUF2 head at the other mediating microtubule binding[1–3,12]. The NDC80–NUF2 coiled-coil contains a break, which makes the rod-like complex highly bendable[13].

Crystallographic structures of both globular head domains have been obtained[2,11], as well as that of a chimaeric version of the human complex containing a minimal coiled-coil, where NDC80 was fused to SPC25 and NUF2 to SPC24 (ref. 12). This 17-nm 'bonsai' complex, which we refer to as Ndc80(bonsai), retained microtubule binding and kinetochore localization. Both NDC80 and NUF2 contain a calponin homology domain (CHD), which is also present in other microtubule binding proteins[14,15]. The unstructured, positively charged 80-amino-acid N-terminal tail of the NDC80 protein is required for high-affinity microtubule binding[2,3,12,16,17], probably by interaction with the acidic carboxy-terminal tails of tubulin (also known as 'E-hooks'). This region of the NDC80 protein, the site of phospho-regulation by the Aurora B kinase[3,12,18], is absent from all crystal structures. The key questions of how the Ndc80 complex binds and remains attached to microtubules during microtubule depolymerization and how this attachment is regulated during mitosis remain unanswered.

Ndc80 binds tubulin with a novel monomeric repeat

We used cryo-electron microscopy to obtain a structure of Ndc80(bonsai) (ref. 12), including the N-terminal tail bound to microtubules. We used an implementation[19] of the iterative helical real space reconstruction method[20], which utilizes reference-free classification to sort helical segments based on symmetry and sample quality (Supplementary Figs 1, 2). Class averages show densities protruding from the microtubule (Supplementary Fig. 1b, top right) with the chevron-like orientation also reported for the *Caenorhabditis elegans* complex[1,21]. Power spectra of class averages show layer lines at 1/40 $Å^{-1}$ (and subsequent orders), corresponding to the spacing of the tubulin monomer (Supplementary Fig. 1b, bottom right), but lack the 1/80 $Å^{-1}$ layer line typically observed for microtubule-binding proteins which recognize the tubulin heterodimer[22–24]. This result suggested that the Ndc80 complex binds to each tubulin monomer.

A helical reconstruction of the *C. elegans* complex suggested alternating binding of the two CHDs to strong and weak sites present in each tubulin dimer[21]. In order to determine the arrangement of the Ndc80 complex on the microtubule lattice without imposing any symmetry or averaging, we obtained tomographic reconstructions of negatively stained microtubules saturated with Ndc80(bonsai) (Supplementary Fig. 1c). Single volume slices allow us to visualize individual tubulin monomers and bound Ndc80 complexes, which are found with a 40 Å spacing within the thickness of a single protofilament. Thus, the human Ndc80 complex binds both α- and β-tubulin monomers.

Microtubule site recognition of the Ndc80 complex

Using a microtubule as a starting reference (Supplementary Fig. 3), we obtained a reconstruction of the Ndc80 complex-bound microtubule at 8.6 Å resolution (Fourier shell correlation (FSC) 0.143 criterion, Supplementary Fig. 4a), allowing us to visualize secondary structure (Fig. 1a; Supplementary Figs 3, 4). The asymmetric units of reconstructed

[1]Biophysics Graduate Group, University of California, Berkeley, California 94720, USA. [2]Department of Experimental Oncology, European Institute of Oncology, 20139 Milan, Italy. [3]Life Sciences Division, Lawrence Berkeley National Laboratory, Berkeley, California 94720, USA. [4]Howard Hughes Medical Institute, Rosenstiel Basic Medical Research Center, Brandeis University, Waltham, Massachusetts 02453, USA. [5]Research Unit of the Italian Institute of Technology at the IFOM-IEO Campus, 20139 Milan, Italy. [6]Howard Hughes Medical Institute, Department of Molecular and Cell Biology, University of California, Berkeley, California 94720, USA.

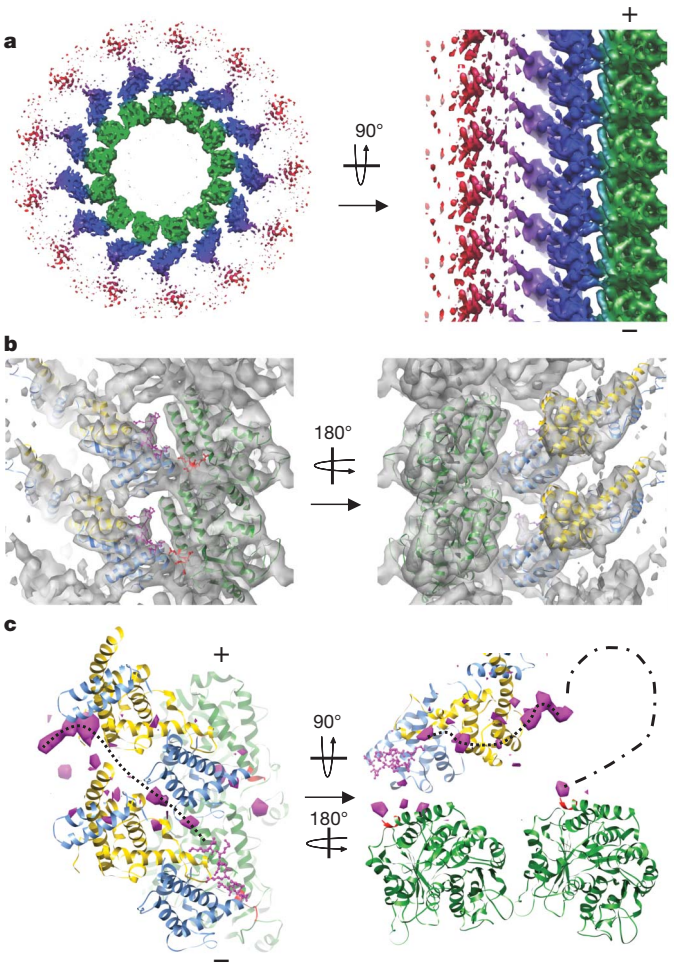

Figure 1 | Structure of the Ndc80 complex–microtubule interface. **a**, End on (from the plus-end) and side views of the microtubule–Ndc80 complex cryo-electron microscopy reconstruction (tubulin, green; NDC80–NUF2 head, blue; disordered SPC24–SPC25 head, red). **b**, Orthogonal views of docked crystal structures (NDC80, blue; NUF2, gold; tubulin, green). In ball and stick representation are residues adjacent to the absent N terminus of NDC80 in Ndc80(bonsai(ΔN)) (magenta), and ordered residues in tubulin preceding the E-hooks (red). The region of the map occupied by NUF2 (right panel) is further from the Ndc80 complex–microtubule interface and thus is of lower resolution. **c**, Orthogonal views of the positive difference density (magenta) between the cryo-electron microscopy reconstruction and the docked crystal structures, contoured at 2.5σ. Dotted lines show a proposed path for the NDC80 N terminus.

13 and 14 protofilament microtubules were essentially identical (Supplementary Fig. 5). Docking of the crystal structures of Ndc80(bonsai) lacking the N terminus of the NDC80 protein—which we refer to as Ndc80(bonsai(ΔN)); ref. 12—and tubulin[25] allowed us to build a pseudo-atomic model of this interface (Fig. 1b). The excellent correspondence between our map and the crystal structure of Ndc80(bonsai(ΔN)) argues against major rearrangements in the globular domains of the complex upon microtubule binding.

The surface of the Ndc80 complex binding the microtubule lattice is minimal, and includes the C-terminal end of helix G and the short helices B and F in the NDC80 protein. This 'toe' recognizes a site between two tubulin monomers, a 'toe-print' present at both intra- and inter-dimer interfaces. The toe-print is composed of the short helix H11′ in one tubulin subunit and the loop connecting helix H8 with β-strand S7 in the other (Fig. 2a, purple and orange, respectively). Superposition of the crystal structures of α- and β-tubulin and multiple-sequence alignments show the toe-print to be highly conserved between the two tubulin monomers (Fig. 2a, bottom), consistent with the ability of the Ndc80 complex to recognize them both. The end of the tubulin crystal structure marking the beginning of the disordered E-hook of tubulin (Fig. 2a, red), required for high-affinity Ndc80 complex binding[1,12], is adjacent to the toe-print, from where we propose it extends and acts as a second, distinct binding site.

The interface we observe is largely in agreement with mutagenesis analysis of NDC80 residues important for binding (for example, K123, K166, H176)[12]. Interestingly, the NUF2 CHD is not in contact with the surface of the microtubule, yet mutations in this region also disrupt binding[12]. The positively charged surface of this domain is approximately 15 Å from the E-hook of a laterally adjacent tubulin monomer and thus could be engaged in an electrostatic interaction.

The Ndc80 toe is a tubulin conformation sensor

During microtubule disassembly, protofilaments bend outwards by kinking of tubulin at intra- and inter-dimer interfaces. In spite of its small size, the toe-print spans a proposed hinge point between tubulin monomers[26] and could thus be disrupted by tubulin bending (Fig. 2a). We therefore hypothesized that the NDC80 toe acts as a sensor of the conformational state of tubulin, and that the complex would bind preferentially to straight protofilaments.

Using co-sedimentation assays, we investigated the ability of Ndc80(bonsai) to bind vinblastine-induced tubulin spirals (Supplementary Fig. 6), a polymer analogous to the peels observed at microtubule ends[27]. Because spirals retain the E-hooks, which make a major contribution to binding affinity, we expected the interaction to be reduced, not eliminated. Indeed, we observed a modest but statistically significant ($P < 0.05$, Student's t-test) reduction in affinity for this form of tubulin versus the straight microtubule conformation (Fig. 2b top, Fig. 2c). We next sought to delineate the relative contributions of the toe versus the N terminus of NDC80 to tubulin binding. Ndc80(bonsai(7D)), a phosphomimetic construct of the seven Aurora B phosphorylation sites confirmed *in vitro*[12] (Online Methods, Supplementary Fig. 7), showed significantly reduced affinity towards the straight microtubule conformation and negligible affinity towards the vinblastine-induced, bent conformation; this reduction reflects the increased relative contribution of the toe-print interaction to affinity when the N terminus–E-hook interaction is impaired (Fig. 3b, c). This result is consistent with a bipartite binding mechanism, with the NDC80 N terminus providing affinity without conformation sensitivity, and the toe providing a smaller contribution to affinity that is exquisitely sensitive to tubulin conformation.

We next investigated the effect of the complex's small bias in affinity towards straight tubulin. We polymerized tubulin into dynamic microtubules, then initiated depolymerization by cooling in the presence or absence of Ndc80(bonsai). Cold-stable microtubules and straight tubulin sheets were observed only in the presence of the Ndc80 complex(Fig. 3d, e). Together, these results are consistent with the Ndc80 complex favouring a straight tubulin conformation, and with this specificity being mediated by the toe. Our studies also indicate that the complex has a stabilizing effect on microtubules.

Ndc80 self-assembles on microtubules

In our cryo-electron microscopy reconstruction, connections appear between Ndc80 complexes along protofilaments (Fig. 1a, b), supporting and explaining the observed cooperative binding of the complex to microtubules[12,17]. We collected tomograms of negatively stained microtubules with non-saturating amounts of Ndc80 complex to test for the presence of Ndc80–Ndc80 complex interactions under more physiological conditions. We found that the complex forms clusters along protofilaments that retain tubulin monomer spacing (Fig. 3a, e; Supplementary Fig. 8). Decoration was heterogeneous, with some microtubules approaching saturation and others almost undecorated (Fig. 3a, Supplementary Fig. 9a); this is a direct manifestation of cooperativity. We do not observe ordered self-association of the complex in the absence of microtubules (Supplementary Fig. 10). Analysis

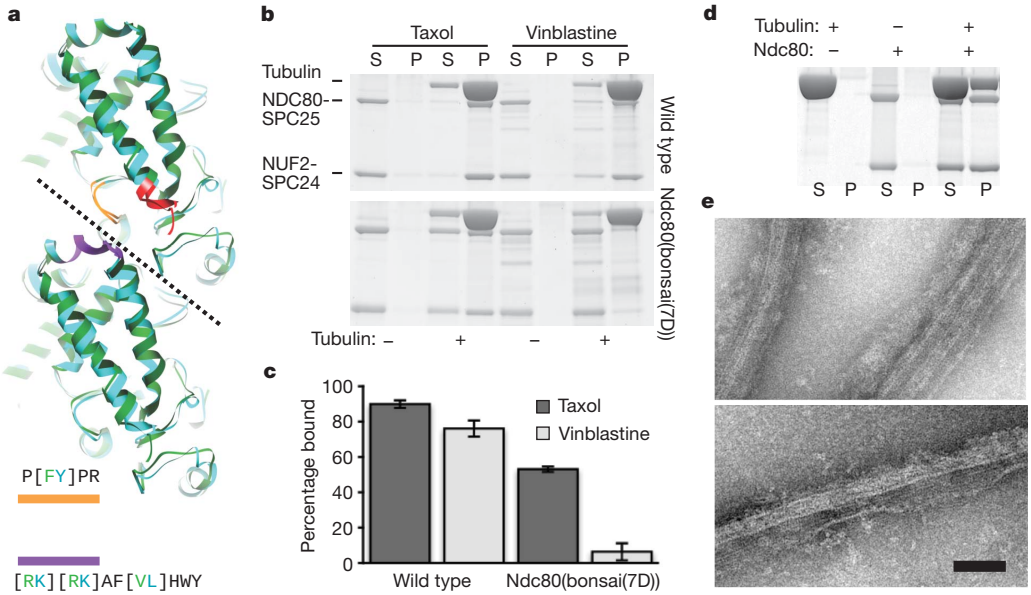

Figure 2 | The NDC80 toe-print is a tubulin conformation sensor. **a**, Superposition of the tubulin intra-dimer and inter-dimer interfaces, viewed from the outside of the microtubule (α-tubulin, green; β-tubulin, blue; ordered residues adjacent to the E-hooks, red; conserved toe-print segments, purple and orange). Consensus sequences are indicated, with deviations between the monomers in parenthesis. **b**, SDS–PAGE of co-sedimentation assays with straight (taxol) and curved (vinblastine) tubulin polymers with the indicated Ndc80(bonsai) constructs. S, supernatant; P, pellet. [Tubulin monomer] = 6 μM, [Ndc80(bonsai)] = 0.5 μM. **c**, Quantification of **b**. Error bars ±s.d., $n = 3$. **d**, SDS–PAGE of co-sedimentation assays after cold-induced depolymerization of dynamic microtubules in the presence and absence of Ndc80(bonsai). **e**, Negative-stain electron microscopy of Ndc80 complex-induced cold-stable microtubules and straight tubulin sheets. Scale bar, 50 nm.

of the pooled distributions of cluster number and size indicates that it is most probable for a complex to be found in a cluster of four molecules or in large clusters of more than ten molecules (Fig. 3i, Supplementary Fig. 9b). Given the reported number (6–8) of Ndc80 complexes per microtubule at the kinetochore, the larger clusters are probably not physiologically relevant[28,29]. Our data are therefore consistent with the formation of two or three clusters per kinetochore microtubule.

Analysis of our docking results shows densities not accounted for by the crystal structures. We attempted to visualize these regions by calculating a difference map between the experimental density map and the docked crystal structures (Fig. 1c; Supplementary Fig. 11). The map shows positive density peaks adjacent to the C-terminal end of the tubulin crystal structure, corresponding to the extension of the H12 helices in each monomer. Stabilization of these residues upon Ndc80 complex binding is consistent with this region of tubulin contributing to affinity[1,12]. Small extra density is also observed by the toe-print. The largest difference density is between the globular domain of NUF2 and the αH–αI helical hairpin of NDC80, with a series of small peaks running along the groove between two longitudinally adjacent complexes, connecting this region with the N-terminal end of the Ndc80(bonsai(ΔN)) crystal structure.

The most parsimonious explanation of this path of density is that it corresponds to the N terminus of NDC80. We propose that the N terminus mediates weak contacts between the globular heads of NDC80 and NUF2 before making a strong contact, corresponding to the major density peak. It could then bind the C terminus of tubulin (necessary for high affinity), probably in an adjacent protofilament. The total mass (80 residues) of the N terminus is not accounted for by these densities, which probably correspond to ordered points of contact formed by this mostly unstructured polypeptide.

The N terminus of Ndc80 mediates regulated self-assembly

In agreement with this proposal, we found that Ndc80(bonsai(ΔN)) was deficient in cluster formation (Fig. 3b, f, i). The presence of some clusters of two complexes suggests that the N terminus is the major but not sole molecular determinant of clustering. We found that Ndc80(bonsai(7D)) showed a clustering phenotype similar to Ndc80(bonsai(ΔN)), with a cluster size of one molecule being the most probable, despite a higher average surface density, and a few clusters of moderate size (Fig. 3c, g, i). We therefore conclude that the N terminus of NDC80 mediates Ndc80–Ndc80 complex interactions, as previously speculated[12], and that phosphorylation at Aurora B sites is capable of modulating this binding.

Next, we dissected the differential contributions of the N terminus to affinity and cooperativity. Subtilisin cleavage of the E-hooks from tubulin significantly reduces the affinity of the Ndc80 complex for microtubules[1,12,17]. As expected, after this treatment we found a significantly lower average surface density of Ndc80 complexes compared to uncleaved microtubules (Fig. 3d, h, i). If the N terminus of NDC80 were only contributing indirectly to cluster formation by increasing microtubule-binding affinity, the cluster size distribution for this condition should be similar to the N terminus mutants. Instead, we observe a most probable cluster size of three molecules, despite an average surface density lower than that of Ndc80(bonsai(7D)) (Fig. 3i). This observation strongly supports our hypothesis that the NDC80 N terminus forms specific intermolecular interactions between complexes on the microtubule surface. It also supports cluster formation occurring after microtubule binding, as the average cluster size on subtilisin-cleaved microtubules is smaller than on uncleaved microtubules.

Role of Ndc80 clusters in mitosis

It was recently demonstrated that Aurora B's activity is governed by spatial localization rather than directly by tension[30], confirming previous proposals[31,32]. On the basis of this finding, we suggest a scheme that starts with phosphorylated Ndc80 complexes in an unattached kinetochore (Fig. 4a)[33]. When the kinetochore encounters a microtubule, individual NDC80-NUF2 heads would initially bind the microtubule through a low-affinity interaction. The bound heads would then escape the Aurora B phosphorylation zone, provided that intra-kinetochore stretching increased as microtubule binding by additional heads allowed the site to come under tension[34]. This could

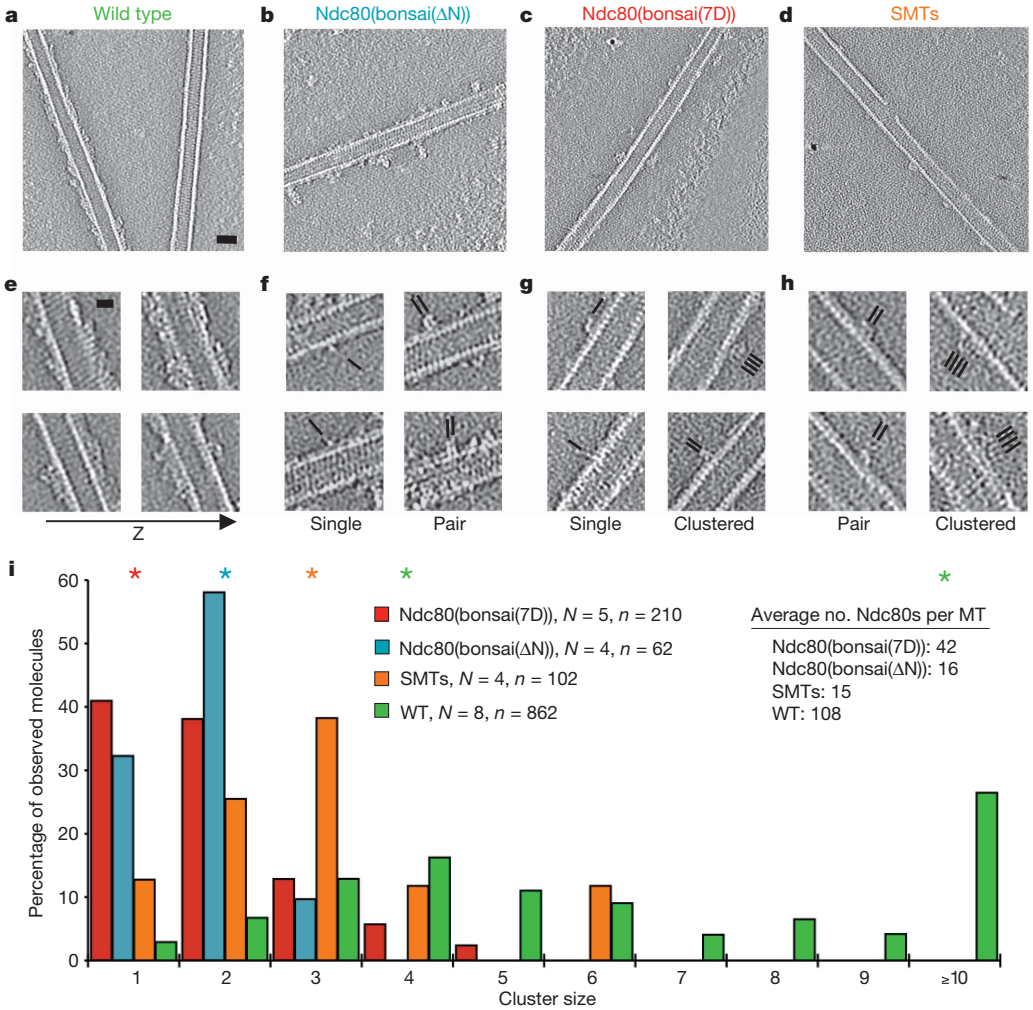

Figure 3 | Cluster formation requires the N terminus of the NDC80 protein. **a–d**, Central slices of tomograms of microtubule-bound Ndc80(bonsai) constructs under subsaturating conditions. Ndc80(bonsai):tubulin monomer ratio was 1:2 for wild-type and subtilisin-cleaved microtubules (SMTs) and 2:1 for NDC80 N terminus mutants. Scale bar, 25 nm; black dots, gold fiducials. **e**, Serial slices of the wild-type reconstruction 4.5 nm apart show cooperative binding and cluster formation only along (not between) protofilaments. Scale bar, 10 nm. **f–h**, Selected views of clusters in Ndc80(bonsai(ΔN)), Ndc80(bonsai(7D)), and SMT reconstructions, respectively. Black lines indicate position and orientation of Ndc80 complexes. **i**, Quantification of cluster size populations. *N*, number of reconstructed microtubule segments; *n*, total number of Ndc80 complexes observed; MT, microtubule; WT, wild type. Asterisks, the most probable cluster size for each of the populations (wild-type has two peaks). See Supplementary Table 1 for pair-wise statistical comparison of these distributions.

occur via straightening of the flexible Ndc80 complex itself[13] (Fig. 4a) or by the stretching of a compliant link in the inner kinetochore[35]. As the phosphorylation zone is cleared, phosphatase activity (possibly KMN-network-localized Protein phosphatase 1; ref. 36) would dephosphorylate the N terminus of NDC80, resulting in the formation of high-affinity Ndc80 complex clusters.

Once assembled, the cluster arrangement is consistent with the complex maintaining load-bearing attachments via biased diffusion[37] (Fig. 4b), as recently proposed on the basis of functional studies[38]. An alternative model, based on shuffling, is also consistent with our data (Supplementary Discussion, Supplementary Fig. 12). Our results support a biased-diffusion model with significant differences from previous studies that presumed either a continuous sleeve[37] or sites uncoupled from the subunit spacing of the microtubule[38]. We propose that Ndc80 complexes oligomerize into linear arrays, resulting in a set of identical, coupled binding sites along protofilaments that match the longitudinal subunit spacing of the microtubule. This arrangement would arise only after the kinetochore comes under tension. Consistent with this hypothesis, outer kinetochore rearrangement on microtubule interaction has been observed *in vivo*[39].

A cluster could diffuse on the microtubule lattice, but its diffusion would become biased at a microtubule end. Thus, a shrinking microtubule would pull the attached chromatid polewards. Cluster diffusion should be facilitated by the 40 Å rather than 80 Å spacing of the Ndc80 complexes, with a shorter distance to the transition state between binding sites during diffusion. Thus, monomer binding may have evolved to enable a biased-diffusion mechanism with sufficiently rapid kinetics (40 Å is the smallest step a microtubule-binding element with a specific footprint can take longitudinally along the microtubule). Our finding that the NDC80 toe serves as a tubulin conformation sensor suggests that microtubule subunit loss is not required to bias diffusion: the curving of protofilaments at a depolymerizing end would suffice[40]. Depolymerizing ends have been observed at metaphase kinetochores *in vivo*, apparently stabilized by attached filaments of unknown identity (Fig. 4b)[41].

Whereas the KMN network and the Ndc80 complex are conserved from yeast to humans, the mechanism of microtubule attachment may not be. We propose that the fungal Ndc80 complex has diverged to act as a coupler to the Dam1 complex, and our structural results, coupled with conservation analysis, suggest a possible binding site for

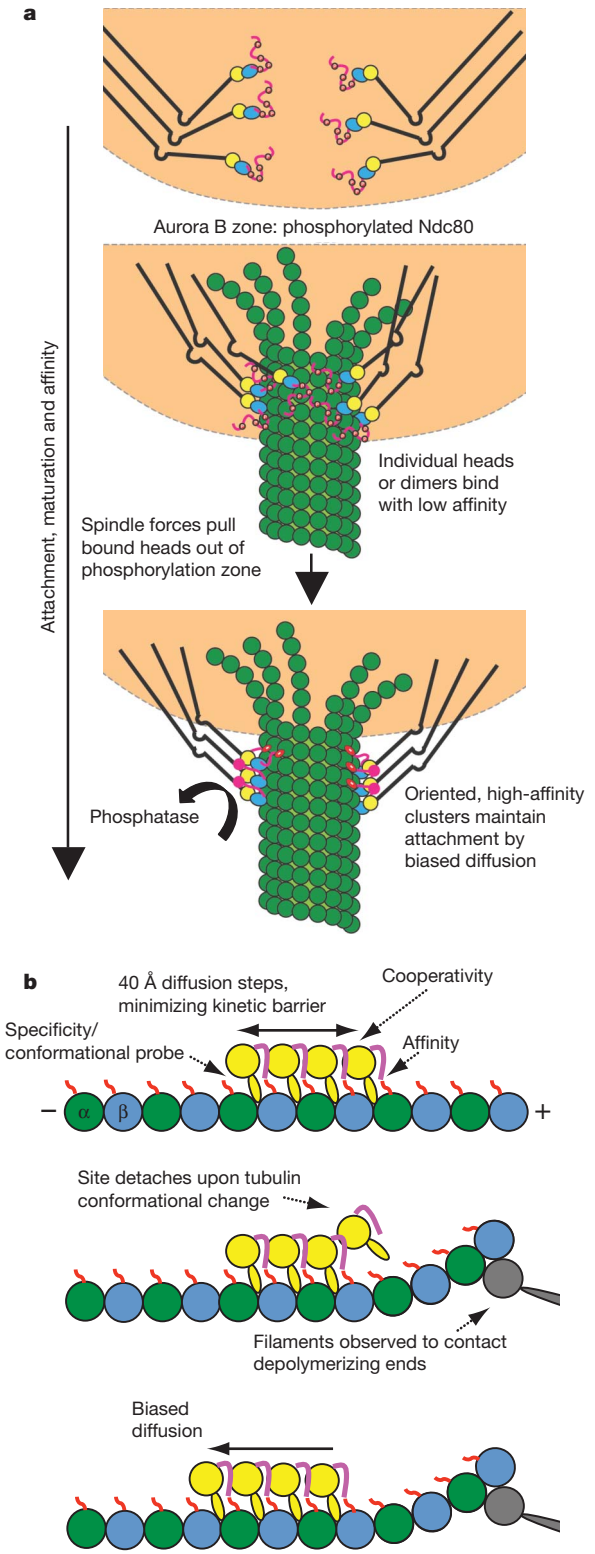

Figure 4 | Proposed models of attachment maturation and biased diffusion. **a**, Cartoon illustrating the phospho-regulated formation of Ndc80 complex clusters *in vivo* concomitant with stable kinetochore–microtubule attachment (colours as Fig. 1b). In this diagram, the assembly of the cluster biased diffusion machinery is regulated by the spatial localization of Aurora B and a counterbalancing phosphatase rather than directly by tension. **b**, Diagrams of the proposed biased diffusion process for coupling chromosome movement to microtubule depolymerization via the Ndc80 complex. Colours as in Fig. 1b, except that the NDC80–NUF2 head is shown in gold and unidentified filaments are shown in grey.

the Dam1 complex on microtubule-bound Ndc80 (Supplementary Discussion, Supplementary Fig. 13).

We have used cryo-electron microscopy and molecular docking to define the interface at the heart of metazoan kinetochore–microtubule attachment. Our studies also demonstrate the microtubule-mediated oligomerization of the Ndc80 complex, which directly involves the Aurora B-regulated N terminus of the NDC80 protein.

METHODS SUMMARY

Cryo-electron microscopy and helical reconstruction. Taxol-stabilized microtubules were decorated with Ndc80(bonsai) after application to glow-discharged C-flat grids (Protochips), then plunge-frozen in ethane slush. Images were collected on Kodak SO-163 film with a Tecnai F20 electron microscope operating at 200 kV at a nominal magnification of 50,000× with a dose of 15 electrons per Å^2. Micrographs were digitized with a Nikon Super CoolScan 8000 scanner with a step size of 6.35 μm. Image processing and projection-matching alignment were carried out using programs from the EMAN, IMAGIC and SPIDER packages, and final refinement and CTF correction was performed with a version of FREALIGN adapted for this work to implement helical symmetry. Visualization and molecular docking was performed with UCSF Chimera. Amplitude-weighted difference maps were calculated using the program DIFFMAP (http://emlab.rose2.brandeis.edu/software). References for all image analysis and visualization software can be found in the Online Methods section.

Tubulin co-sedimentation assays. Tubulin polymerized with or without conformation-stabilizing drugs was mixed with Ndc80(bonsai), then layered on to a 50% glycerol cushion supplemented with additives and pelleted by ultracentrifugation in a Beckman TLA100 rotor at 312,530*g* for 10 min (ref. 12). Supernatant and pellet fractions were analysed by SDS–polyacrylamide gel electrophoresis (SDS–PAGE).

Electron tomography. Samples were prepared on C-flat grids augmented with a continuous carbon layer, and stained with uranyl formate. Tilt series were collected on 2k × 2k CCD cameras using a JEOL 3100 microscope operating at 300 kV with the SerialEM package, or a Phillips CM200 microscope operating at 200 kV with Digital Micrograph (Gatan). Processing was carried out with programs from the EMAN, SPIDER and IMOD software packages. References for all image analysis software can be found in the Online Methods section.

Full Methods and any associated references are available in the online version of the paper at www.nature.com/nature.

Received 10 February; accepted 13 August 2010.

1. Cheeseman, I. M., Chappie, J. S., Wilson-Kubalek, E. M. & Desai, A. The conserved KMN network constitutes the core microtubule-binding site of the kinetochore. *Cell* **127,** 983–997 (2006).
2. Wei, R. R., Al-Bassam, J. & Harrison, S. C. The Ndc80/HEC1 complex is a contact point for kinetochore-microtubule attachment. *Nature Struct. Mol. Biol.* **14,** 54–59 (2007).
3. DeLuca, J. G. *et al.* Kinetochore microtubule dynamics and attachment stability are regulated by Hec1. *Cell* **127,** 969–982 (2006).
4. Martin-Lluesma, S., Stucke, V. M. & Nigg, E. A. Role of Hec1 in spindle checkpoint signaling and kinetochore recruitment of Mad1/Mad2. *Science* **297,** 2267–2270 (2002).
5. DeLuca, J. G. *et al.* Nuf2 and Hec1 are required for retention of the checkpoint proteins Mad1 and Mad2 to kinetochores. *Curr. Biol.* **13,** 2103–2109 (2003).
6. Kemmler, S. *et al.* Mimicking Ndc80 phosphorylation triggers spindle assembly checkpoint signalling. *EMBO J.* **28,** 1099–1110 (2009).
7. Chen, Y., Riley, D. J., Chen, P. L. & Lee, W. H. HEC, a novel nuclear protein rich in leucine heptad repeats specifically involved in mitosis. *Mol. Cell. Biol.* **17,** 6049–6056 (1997).
8. Wigge, P. A. *et al.* Analysis of the Saccharomyces spindle pole by matrix-assisted laser desorption/ionization (MALDI) mass spectrometry. *J. Cell Biol.* **141,** 967–977 (1998).
9. Wei, R. R., Sorger, P. K. & Harrison, S. C. Molecular organization of the Ndc80 complex, an essential kinetochore component. *Proc. Natl Acad. Sci. USA* **102,** 5363–5367 (2005).
10. Ciferri, C. *et al.* Architecture of the human ndc80-hec1 complex, a critical constituent of the outer kinetochore. *J. Biol. Chem.* **280,** 29088–29095 (2005).
11. Wei, R. R. *et al.* Structure of a central component of the yeast kinetochore: the Spc24p/Spc25p globular domain. *Structure* **14,** 1003–1009 (2006).
12. Ciferri, C. *et al.* Implications for kinetochore-microtubule attachment from the structure of an engineered Ndc80 complex. *Cell* **133,** 427–439 (2008).
13. Wang, H. W. *et al.* Architecture and flexibility of the yeast Ndc80 kinetochore complex. *J. Mol. Biol.* **383,** 894–903 (2008).
14. Hayashi, I., Wilde, A., Mal, T. K. & Ikura, M. Structural basis for the activation of microtubule assembly by the EB1 and p150Glued complex. *Mol. Cell* **19,** 449–460 (2005).
15. Slep, K. C. & Vale, R. D. Structural basis of microtubule plus end tracking by XMAP215, CLIP-170, and EB1. *Mol. Cell* **27,** 976–991 (2007).

16. Guimaraes, G. J., Dong, Y., McEwen, B. F. & Deluca, J. G. Kinetochore-microtubule attachment relies on the disordered N-terminal tail domain of Hec1. *Curr. Biol.* **18,** 1778–1784 (2008).
17. Miller, S. A., Johnson, M. L. & Stukenberg, P. T. Kinetochore attachments require an interaction between unstructured tails on microtubules and Ndc80(Hec1). *Curr. Biol.* **18,** 1785–1791 (2008).
18. Cheeseman, I. M. *et al.* Phospho-regulation of kinetochore-microtubule attachments by the Aurora kinase Ipl1p. *Cell* **111,** 163–172 (2002).
19. Ramey, V. H., Wang, H. W. & Nogales, E. Ab initio reconstruction of helical samples with heterogeneity, disorder and coexisting symmetries. *J. Struct. Biol.* **167,** 97–105 (2009).
20. Egelman, E. H. The iterative helical real space reconstruction method: surmounting the problems posed by real polymers. *J. Struct. Biol.* **157,** 83–94 (2007).
21. Wilson-Kubalek, E. M., Cheeseman, I. M., Yoshioka, C., Desai, A. & Milligan, R. A. Orientation and structure of the Ndc80 complex on the microtubule lattice. *J. Cell Biol.* **182,** 1055–1061 (2008).
22. Mizuno, N., Narita, A., Kon, T., Sutoh, K. & Kikkawa, M. Three-dimensional structure of cytoplasmic dynein bound to microtubules. *Proc. Natl Acad. Sci. USA* **104,** 20832–20837 (2007).
23. Hoenger, A. & Gross, H. Structural investigations into microtubule-MAP complexes. *Methods Cell Biol.* **84,** 425–444 (2008).
24. des Georges, A. *et al.* Mal3, the *Schizosaccharomyces pombe* homolog of EB1, changes the microtubule lattice. *Nature Struct. Mol. Biol.* **15,** 1102–1108 (2008).
25. Löwe, J., Li, H., Downing, K. H. & Nogales, E. Refined structure of alpha beta-tubulin at 3.5 A resolution. *J. Mol. Biol.* **313,** 1045–1057 (2001).
26. Wang, H. W. & Nogales, E. Nucleotide-dependent bending flexibility of tubulin regulates microtubule assembly. *Nature* **435,** 911–915 (2005).
27. Wilson, L., Jordan, M. A., Morse, A. & Margolis, R. L. Interaction of vinblastine with steady-state microtubules *in vitro*. *J. Mol. Biol.* **159,** 125–149 (1982).
28. Joglekar, A. P., Bouck, D. C., Molk, J. N., Bloom, K. S. & Salmon, E. D. Molecular architecture of a kinetochore-microtubule attachment site. *Nature Cell Biol.* **8,** 581–585 (2006).
29. Joglekar, A. P. *et al.* Molecular architecture of the kinetochore-microtubule attachment site is conserved between point and regional centromeres. *J. Cell Biol.* **181,** 587–594 (2008).
30. Liu, D., Vader, G., Vromans, M. J., Lampson, M. A. & Lens, S. M. Sensing chromosome bi-orientation by spatial separation of aurora B kinase from kinetochore substrates. *Science* **323,** 1350–1353 (2009).
31. Tanaka, T. U. *et al.* Evidence that the Ipl1-Sli15 (Aurora kinase-INCENP) complex promotes chromosome bi-orientation by altering kinetochore-spindle pole connections. *Cell* **108,** 317–329 (2002).
32. Andrews, P. D. *et al.* Aurora B regulates MCAK at the mitotic centromere. *Dev. Cell* **6,** 253–268 (2004).
33. Santaguida, S. & Musacchio, A. The life and miracles of kinetochores. *EMBO J.* **28,** 2511–2531 (2009).
34. Maresca, T. J. & Salmon, E. D. Intrakinetochore stretch is associated with changes in kinetochore phosphorylation and spindle assembly checkpoint activity. *J. Cell Biol.* **184,** 373–381 (2009).
35. Wan, X. *et al.* Protein architecture of the human kinetochore microtubule attachment site. *Cell* **137,** 672–684 (2009).
36. Liu, D. *et al.* Regulated targeting of protein phosphatase 1 to the outer kinetochore by KNL1 opposes Aurora B kinase. *J. Cell Biol.* **188,** 809–820 (2010).
37. Hill, T. L. Theoretical problems related to the attachment of microtubules to kinetochores. *Proc. Natl Acad. Sci. USA* **82,** 4404–4408 (1985).
38. Powers, A. F. *et al.* The Ndc80 kinetochore complex forms load-bearing attachments to dynamic microtubule tips via biased diffusion. *Cell* **136,** 865–875 (2009).
39. Dong, Y., Vanden Beldt, K. J., Meng, X., Khodjakov, A. & McEwen, B. F. The outer plate in vertebrate kinetochores is a flexible network with multiple microtubule interactions. *Nature Cell Biol.* **9,** 516–522 (2007).
40. Lombillo, V. A., Stewart, R. J. & McIntosh, J. R. Minus-end-directed motion of kinesin-coated microspheres driven by microtubule depolymerization. *Nature* **373,** 161–164 (1995).
41. McIntosh, J. R. *et al.* Fibrils connect microtubule tips with kinetochores: a mechanism to couple tubulin dynamics to chromosome motion. *Cell* **135,** 322–333 (2008).

Supplementary Information is linked to the online version of the paper at www.nature.com/nature.

Acknowledgements We are grateful to K. H. Downing for supporting the work carried out by D.A.B., to C. Ciferri for his knowledge and advice about the Ndc80 complex and critical reading of the manuscript, and to P. Grob and S. Lipscomb for electron-microscopy and computer support, respectively. We also acknowledge D. Typke and B. Glaeser for advice on data collection, and C. Sindelar for discussion of data processing strategies. This work was funded by a grant from the National Institute of General Medical Sciences (E.N.). E.N. and N.G. are Howard Hughes Medical Institute Investigators.

Author Contributions G.M.A. performed research. G.M.A. and V.H.R. developed data processing tools. G.M.A. and S.P. generated and purified Ndc80(bonsai) mutants. D.A.B. generated the tomograms displayed in Supplementary Fig. 1. N.G. adapted Frealign software for helical samples and generated the final refined reconstruction. G.M.A. and E.N. designed research. All authors analysed data and discussed the results. G.M.A., A.M. and E.N. wrote the Article.

Author Information The cryo-electron microscopy density map and coordinates of the docking model have been deposited at the EMDB and PDB under accession numbers 5223 and 3IZ0, respectively. Reprints and permissions information is available at www.nature.com/reprints. The authors declare no competing financial interests. Readers are welcome to comment on the online version of this article at www.nature.com/nature. Correspondence and requests for materials should be addressed to E.N. (enogales@lbl.gov).

METHODS

Mutagenesis. Ndc80(bonsai) point mutations were generated using standard procedures for site-directed mutagenesis. The Ndc80(bonsai(7D)) mutant was generated as follows: Synonymous mutations were performed that destroyed the StuI restriction site at base pair (bp) 81–86 of the NDC80–SPC25 protein coding sequence and subsequently reintroduced it at bp 250–255. An NdeI restriction site was also created 5′ to the beginning of the coding sequence. This construct thus features a swappable NDC80 N terminus cassette. A sequence coding for the seven *in vitro* verified[12] Aurora B phosphorylation sites mutated to aspartic acid (S4D, S8D, S15D, S44D, S55D, S62D, S69D) was synthesized (GENEART) and cloned into the swappable N terminus construct using standard protocols.

Biochemical sample preparation. Ndc80(bonsai) complex was purified as described[12]. 10 mg ml^{-1} bovine brain tubulin (Cytoskeleton) was polymerized in CB1 buffer (80 mM PIPES pH 6.8, 1 mM EGTA, 1 mM $MgCl_2$, 1 mM GTP, 10% glycerol) for 15 min at 37 °C before addition of 160 μM taxol, followed by 30–60 min of further incubation. We have found this procedure primarily produces 13 and 14 protofilament microtubules. Microtubules were pelleted at 17,000*g* in a tabletop microcentrifuge for 20 min, then resuspended in room temperature EM buffer (80 mM PIPES pH 6.8, 1 mM EGTA, 1 mM $MgCl_2$, 1 mM DTT, 0.05% Nonidet P-40) supplemented with 160 μM taxol. Tubulin concentration was assayed by A_{280} after depolymerization on ice with 50 mM $CaCl_2$.

Ndc80(bonsai) at 2 mg ml^{-1} was rapidly thawed before storage on ice, diluted 1:1 with EM buffer, then desalted into EM buffer using a Zeba spin desalting column (Pierce). The removal of salt resulted in a rapid precipitation of the sample, which was clarified by ultracentrifugation in a Beckman TLA100 rotor for 20 min at 61,734*g* at 4 °C. The sample was then warmed to 25 °C for approximately 15 min before electron microscopy grid preparation, which resulted in a second round of precipitation/self-association. Analysis of the sample at this stage by negative-stain electron microscopy did not reveal any ordered assemblies (Supplementary Fig. 10). The sample was once again clarified for 3 min at 17,000*g* in a tabletop microcentrifuge. Protein concentration was estimated with the Coomassie Plus protein assay reagent (Pierce) using bovine serum albumin (BSA) as a reference. It is notable that the amount of precipitation was dependent on the state of the NDC80 N terminus: the Ndc80(bonsai(ΔN)) and Ndc80(bonsai(7D)) constructs were significantly more stable under low-salt conditions.

Cryo-sample preparation. C-flat grids (Protochips) were glow-discharged using an Edwards Carbon Evaporator. Taxol-stabilized microtubules were diluted to 0.25 mg ml^{-1} in EM buffer supplemented with 20 μM taxol, and 2 μl was applied to the grid in the humidity chamber of a Vitrobot (Maastricht Instruments). After 1 min, 4 μl of ~0.7 mg ml^{-1} Ndc80(bonsai) was added, corresponding to a molar ratio of ~2:1 Ndc80 complex:tubulin monomer, and incubated for 1 min. The grid was then briefly blotted before a second 4 μl addition of Ndc80 complex and 1 min incubation. 2 μl was then removed from the grid, which was then blotted for 2 s and plunged into ethane slush. This protocol is essentially similar to that used for visualization of the *C. elegans* complex[21], with minor modification.

Cryo-electron microscopy. 100 micrographs were collected on Kodak SO-163 film with a Tecnai F20 electron microscope operating at 200 kV at a nominal magnification of 50,000× with a dose of 15 electrons per Å^2, between 1.2 μm and 2.2 μm underfocus. Micrographs were digitized with a Nikon Super CoolScan 8000 scanner with a step size of 6.35 μm. After digitization, the power spectra of carbon present in each image was examined, and images lacking Thon rings to at least 8 Å were excluded.

Image processing and IHRSR. We carried out helical processing essentially as described[19], with some modifications. Unless otherwise indicated, all processing steps were implemented with the SPIDER package[42]. The pixel size of the digitized micrographs was calibrated to be 1.24 Å by examination of the power spectrum of samples of tobacco mosaic virus (TMV) imaged under identical conditions. CTF parameters were estimated for each image using the program CTFFIND3[43]. Images were divided into three approximate defocus groups (1.2 μm, 1.7 μm, 2.2 μm). Segments 768 pixels long were extracted from the micrographs with the helix option in BOXER[44], using 90% overlap[20]. Pixel intensities were normalized, and large-scale gradients in intensity due to variations in ice thickness were subtracted. A two-dimensional Wiener filter was then applied to each segment, with the intention of aiding the detection of highly ordered segments, which should diffract to high resolution. Subsequent experience has demonstrated that this step is not necessary for robust classification based on helical quality, and may in fact be detrimental in cases with a low signal-to-noise ratio in the low spatial frequency regime, as amplification of high-resolution spatial frequency components in raw images drives alignment based on noise rather than signal. The segments were then masked such that each image contained approximately 2 turns of the 1-start helix, corresponding to 78 asymmetric units, and decimated threefold to a pixel size of 3.72 Å.

We then subjected the data to reference-free two-dimensional classification as described[19]. This method successfully sorts segments on the basis of protofilament number and helical quality, as is apparent in Supplementary Fig. 2. As microtubules can incorporate varying numbers of protofilaments *in vitro*[45], and segments vary in their quality, this method is used as an alternative to assessing each individual microtubule by manual inspection of Moiré patterns and power spectra. Out of an initial set of 10,253 segments, only 1,475 were members of classes that corresponded to well-ordered 13 protofilament microtubules and were selected for further processing.

Segments from defocus groups were combined before IHRSR with SPIDER. Using a naked microtubule as a reference, the reconstruction converged after 10 rounds of refinement. Particles with cross-correlation scores less than one standard deviation below the mean were excluded, corresponding to approximately 30% of the data. The final refined helical parameters correspond to a rise of 42.7 Å per tubulin monomer. This is slightly greater than the reported value of 41.7 Å for taxol-stabilized microtubules[46], but could result from an error in our pixel size estimation, as TMV was not observed *in situ*. The full three-start symmetry of the microtubule was applied after refinement was complete by real-space averaging. The resolution of the reconstruction at this stage was limited to approximately 20 Å ('bronze' reconstruction, Supplementary Fig. 3), as filtering the volume at higher resolution did not reveal any additional features.

This limit in resolution was found to be at least partially due to limited pixel sampling. With no further alignment of the particles, simply reducing the decimation factor of the original CTF-corrected data from threefold to twofold (2.48 Å per pixel) resulted in a discrete jump in resolution, to approximately 12–15 Å resolution ('silver' reconstruction, Supplementary Fig. 3). The mask on each particle was removed at this stage, increasing the number of asymmetric units incorporated into the reconstruction, as not all segments incorporated into the reconstruction were from adjacent positions in microtubule filaments. Approximately 50,000 asymmetric units were incorporated at this stage, and secondary structure elements began to be visualized when a B-factor of −450 Å^2 was applied with the program bfactor (http://emlab.rose2.brandeis.edu/software) using the cosine edge mask option with a radius of 8.5 Å. This model was used as the input for final refinement in Frealign.

Final refinement with Frealign. We used the computer program Frealign[47] to refine our reconstruction. Frealign was originally designed to work with single particle images. To work with helical particles, we implemented a helical symmetry operator (symmetry operator H in Frealign) and followed a reconstruction algorithm described previously[48]. Masking of the helical sections is done using a rectangular mask that is aligned with the helical axis of the particle in each section. Using the helical symmetry operator, a set of Euler angles and shifts producing equivalent views for each section can be calculated. Using this set of alignment parameters, each section is inserted multiple times into the reconstruction. The number of insertions is matched to the degree of overlap between helical sections such that it corresponds to the number of symmetry-related subunits contained in the non-overlapping part of each section. In the case of the Ndc80 complex-decorated microtubules, the unique, non-overlapping area of the filament was chosen to contain approximately one helical turn of 13 subunits. In addition to this, the 3-start helical symmetry of the 13 protofilament microtubule increased the number of unique subunits per segment threefold, to 39. Therefore, in the present case, each helical segment is inserted into the three-dimensional reconstruction 39 times using Euler angles and shifts that represent equivalent views of the particle. The final reconstruction is masked using a cylindrical mask with user-defined radius, and the helical symmetry is imposed in real space (option BEAUTIFY in Frealign) to remove the small density gradient along the helical axis due to the reconstruction algorithm[48].

For the refinement of Euler angles and shifts for each helical section, the reference projections from the helical reference are masked with a soft-edged mask to reset the image density to background level in a 10% margin near the edges of the image. This is necessary to avoid truncation of reference projections at the edges when applying the small shifts typically observed during alignment. Furthermore, the refinement is carried out using the weighted correlation coefficient[49], but without the use of the absolute value. For helical structures, the low-resolution correlation terms are essentially insensitive to shifts along the helical axis and, therefore, if the absolute value is used, the high-resolution layer lines may be rendered out of phase during alignment. Finally, the Euler angles describing in-plane and out-of-plane alignments of each section are restrained as previously described[50], but using separate statistics for each segment. No restraints were used for the shifts. The final reconstruction was scaled to the same amplitude profile as the input reconstruction, and is shown in gold in Supplementary Fig. 3.

Difference map calculation. The experimental map was segmented, and an appropriate number of Ndc80(bonsai(ΔN)) and tubulin crystal structures were docked into the map to approximately account for the total mass with UCSF

Chimera[51]. These crystal structures were converted into SPIDER volume format using the CP FROM PDB command, then filtered to 8 Å resolution. Although this procedure retained the orientation of the crystal structures relative to each other, this volume had to be re-docked into the experimental map, which was accomplished using a cross-correlation search with SPIDER. The amplitude-weighted difference map was calculated using the program DIFFMAP (http://emlab.rose2.brandeis.edu/diffmap). Amplitude weighting was critical for a meaningful comparison, as the amplitudes of the volume derived from the crystal structures were down-weighted several hundred fold in all resolution shells.

Tubulin co-sedimentation assays. For biochemical assays Ndc80(bonsai) proteins were desalted into binding buffer (80 mM PIPES pH 6.8, 1 mM EGTA, 1 mM $MgCl_2$, 1 mM DTT, 5% sucrose). We found that this buffer increased the solubility of the protein in the absence of salt while allowing for accurate determination of protein concentration by A_{280}. The phenyl group of Nonidet P-40 results in significant absorbance of EM buffer at 280 nm, which is refractory to reproducible protein concentration measurement by this method. The presence of sucrose significantly reduces contrast in the electron microscope, and thus binding buffer was not used for any of the imaging experiments shown. In control imaging experiments, we have found no differences in Ndc80 complex–microtubule interactions or tubulin polymer behaviour between the two buffers (data not shown).

To generate vinblastine spirals, we diluted tubulin stored in CB1 buffer to 3 mg ml^{-1} in binding buffer supplemented with 1 mM vinblastine sulphate (Sigma). After two hours incubation at 25 °C, robust formation of spiral aggregates was observed (Supplementary Fig. 6).

Taxol microtubules or vinblastine spirals (6 μM tubulin monomer) and Ndc80(bonsai) proteins (0.5 μM) were mixed in a 50 μl reaction volume and incubated at 25 °C for 15 min in the presence of 20 μM taxol or 1 mM vinblastine. The binding reactions were layered on to a 100 μl 50% glycerol cushion containing buffer components and the appropriate drug and polymers were pelleted by ultracentrifugation at 312,530*g*. in a Beckman TLA 100 rotor for 10 min at 25 °C, essentially as described[12]. Supernatant and pellet fractions were collected and precipitated in 90% ethanol at −20 °C for 16 h before analysis by SDS–PAGE. Gels were stained with Flamingo fluorescent gel stain (Bio-Rad), and imaged with a Typhoon Trio (GE Healthcare). Apparent slight degradation of the Ndc80 complex was observed in the presence of 1 mM vinblastine sulphate (Fig. 2b), but this did not cause spurious pelleting of the complex in the absence of tubulin. Quantification was performed with ImageJ[52].

To test for cold stabilization, 10 mg ml^{-1} tubulin in CB1 buffer was polymerized for 45 min at 37 °C. A binding reaction containing Ndc80(bonsai) in binding buffer was set up on ice, and then heated to 37 °C for 1 min. Dynamic microtubules were then added to this reaction for a final concentration of 20 μM tubulin and 3.3 μM NDC80 and incubated at 37 °C for 10 min. The reaction was then shifted to ice for 30 min, and subsequently analysed by pelleting assay as above, except ultracentrifugation was performed at 4 °C.

To analyse the outcomes of the described experiments by negative stain electron microscopy, we repeated them substituting EM buffer for binding buffer. Samples were prepared on continuous carbon grids, stained with 2% uranyl acetate, and imaged on a 1k × 1k CCD camera with a Tecnai T12 electron microscope operating at 120 kV between approximately 1 μm and 2 μm underfocus.

Negative stain sample preparation for tomography. Samples were prepared as described for cryo-electron microscopy, except that the grids were augmented with a layer of thin carbon and treated with gold fiducial markers (British BioCell International) before sample application. To achieve sub-saturating binding, wild-type Ndc80(bonsai) was diluted to 0.15 mg ml^{-1} and only a single application was performed, corresponding to a 1:2 Ndc80 complex:tubulin monomer ratio. To generate SMTs, taxol-stabilized microtubules were digested with 1.5 μM subtilisin A (Calbiochem) in EM buffer for 30 min at 37 °C. The reaction was stopped with 2 mM PMSF, and the SMTs were pelleted and resuspended in EM buffer before sample preparation.

To achieve saturation in the case of wild-type and to observe binding in the case of Ndc80(bonsai(ΔN)) and Ndc80(bonsai(7D)), double-application of 0.6–0.7 mg ml^{-1} Ndc80 complex was performed, corresponding to a 2:1 Ndc80 complex:tubulin monomer ratio. Samples were stained with 2% uranyl formate.

Electron tomography and cluster quantification. The tomograms displayed in Supplementary Fig. 1 were derived from tilt series collected on a 2k × 2k CCD camera from −60° to 60° using a JEOL 3100 microscope operating at 300 kV at approximately 2 μm underfocus with a nominal magnification of 40,000×. The acquisition was performed semi-automatically using a version of SerialEM (http://bio3d.colorado.edu) adapted for operating JEOL microscopes. Raw tomographic image stacks were aligned either manually with the eTomo suite of programs, or automatically using the software RAPTOR[53]. Tomographic reconstructions were constructed using the eTomo suite of programs and visualized using the IMOD software package[54].

The tomograms displayed in Fig. 3 were derived from tilt series collected from −65° to 65° on a 2k × 2k CCD camera using a Phillips CM200 microscope operating at 200 kV at approximately 2.5 μm underfocus at a nominal magnification of 39,000×. Images were filtered to 25–30 Å, before the first phase-inversion of the contrast-transfer function, and decimated twofold before reconstruction as described above.

Cluster quantification was performed by manual inspection of the reconstructions. The raw data are shown in Supplementary Fig. 9b, and consist of number of counts versus cluster size. Clusters ≥10 molecules in size were ignored in the case of the wild type, as we believe they are not physiologically relevant and would bias comparisons between the distributions towards spurious difference. Pair-wise comparisons were performed using Welch's *t*-test[55], which is appropriate for samples featuring both different numbers of observations and possibly unequal variances (which the unbiased estimator of the variance of the distributions suggested in this case), and *P*-values are shown in Supplementary Table 1. In all but one of the cases $P < 0.0015$, suggesting that the data derived from each of the conditions shown in Fig. 3 and Supplementary Fig. 9 do indeed sample different distributions. The exception was Ndc80(bonsai(7D)) versus Ndc80(bonsai(ΔN)), where we find a probability of 0.61 of sampling the same distribution. This supports our assertion that these two mutants phenocopy each other.

Conservation analysis and structure alignments. We performed multiple-sequence alignments using CLUSTALW2[56], and mapped this analysis on to the Ndc80(bonsai(ΔN)) crystal structure using the CONSURF server[57]. The alignments included 48 fungi sequences and 39 metazoan sequences in the case of NDC80 and 52 fungi sequences and 22 metazoan sequences in the case of NUF2, and are available on request. Sequences of α- and β-tubulin from six representative organisms (*Saccharomyces cerevisiae*, *Caenorhabditis elegans, Drosophila melanogaster*, *Xenopus laevis, Bos taurus* and *Homo sapiens*) were compared. Since the Ndc80(bonsai(ΔN)) crystal structure is of the human complex, fungal sequences had to be threaded on to the structure by alignment with the human sequence. As we observe a similar pattern of conservation at the NDC80 toe, we believe this procedure was successful. All superpositions of crystal structures were performed with the MatchMaker function in UCSF Chimera[51].

42. Frank, J. *et al.* SPIDER and WEB: processing and visualization of images in 3D electron microscopy and related fields. *J. Struct. Biol.* **116,** 190–199 (1996).
43. Mindell, J. A. & Grigorieff, N. Accurate determination of local defocus and specimen tilt in electron microscopy. *J. Struct. Biol.* **142,** 334–347 (2003).
44. Ludtke, S. J., Baldwin, P. R. & Chiu, W. EMAN: semiautomated software for high-resolution single-particle reconstructions. *J. Struct. Biol.* **128,** 82–97 (1999).
45. Wade, R. H., Chretien, D. & Job, D. Characterization of microtubule protofilament numbers. How does the surface lattice accommodate? *J. Mol. Biol.* **212,** 775–786 (1990).
46. Arnal, I. & Wade, R. H. How does taxol stabilize microtubules? *Curr. Biol.* **5,** 900–908 (1995).
47. Grigorieff, N. FREALIGN: high-resolution refinement of single particle structures. *J. Struct. Biol.* **157,** 117–125 (2007).
48. Sachse, C. *et al.* High-resolution electron microscopy of helical specimens: a fresh look at tobacco mosaic virus. *J. Mol. Biol.* **371,** 812–835 (2007).
49. Stewart, A. & Grigorieff, N. Noise bias in the refinement of structures derived from single particles. *Ultramicroscopy* **102,** 67–84 (2004).
50. Chen, J. Z. *et al.* Molecular interactions in rotavirus assembly and uncoating seen by high-resolution cryo-EM. *Proc. Natl Acad. Sci. USA* **106,** 10644–10648 (2009).
51. Goddard, T. D., Huang, C. C. & Ferrin, T. E. Software extensions to UCSF chimera for interactive visualization of large molecular assemblies. *Structure* **13,** 473–482 (2005).
52. Abramoff, M. D., Magelhaes, P. J. & Ram, S. J. Image Processing with ImageJ. *Biophotonics International* **11,** 36–42 (2004).
53. Amat, F. *et al.* Markov random field based automatic image alignment for electron tomography. *J. Struct. Biol.* **161,** 260–275 (2008).
54. Kremer, J. R., Mastronarde, D. N. & McIntosh, J. R. Computer visualization of three-dimensional image data using IMOD. *J. Struct. Biol.* **116,** 71–76 (1996).
55. Welch, B. L. The generalisation of student's problems when several different population variances are involved. *Biometrika* **34,** 28–35 (1947).
56. Larkin, M. A. *et al.* Clustal W and Clustal X version 2.0. *Bioinformatics* **23,** 2947–2948 (2007).
57. Landau, M. *et al.* Consurf 2005: the projection of evolutionary conservation scores of residues on protein structures. *Nucleic Acids Res.* **33,** W299–302 (2005).